PHYSICAL REVIEW B **79**, 155426 (2009)

Phase diagrams and optical properties of phosphide, arsenide, and antimonide binary and ternary III-V nanoalloys

G. Guisbiers,[1,*] M. Wautelet,[2] and L. Buchaillot[1]
[1]IEMN, CNRS-UMR8520, Scientific City, Avenue Henri Poincaré, Boîte Postale 60069, 59652 Villeneuve d'Ascq, France
[2]Physics of Condensed Matter, University of Mons-Hainaut, 23 Avenue Maistriau, 7000 Mons, Belgium
(Received 19 February 2009; published 16 April 2009)

We report a theoretical investigation, at the nanoscale, free of any adjustable parameters, concerning the size, shape, composition, and segregation effects on the melting temperature and energy band gap of zinc-blende III-V semiconductors. The corresponding nanophase diagram is established. From it, the composition and segregation effects on the energy band gap of the ternary semiconducting nanoalloy are deduced. Moreover, the liquid surface energies for AlP, GaP, AlAs, and AlSb have been calculated (0.566 ± 0.060, 0.510 ± 0.060, 0.506 ± 0.060 J/m^2, and 0.441 ± 0.060 J/m^2, respectively). The information obtained in this study can be used to tune the thermo-optical properties of III-V nanomaterials in nano-optoelectronics.

DOI: 10.1103/PhysRevB.79.155426 PACS number(s): 73.22.−f, 65.80.+n, 78.67.−n, 81.05.Ea

I. INTRODUCTION

The semiconducting alloys $A_x^{\mathrm{III}}B_{1-x}^{\mathrm{V}}$, $A_x^{\mathrm{III}}B_{1-x}^{\mathrm{III}}C^{\mathrm{V}}$, and $A^{\mathrm{III}}B_x^{\mathrm{V}}C_{1-x}^{\mathrm{V}}$ composed of elements (A, B, and C) from groups III and V of the periodic table, more generally called III-V, are an important class of materials.[1,2] A large variety of materials properties may be obtained by varying the composition, x, of the III/V elements involved in the alloy. These alloys are used in systems for which they outperform silicon because of better-suited materials properties. For example, the high electron mobility of GaAs is advantageous in microwave devices and the small band gap of InSb is suitable in infrared applications. Other systems as light-emitting diodes (LEDs) (Ref. 3) which require a well-tuned energy band gap can only be fabricated with semiconducting alloys.

A large number of these III-V semiconducting compounds exhibit complete solid miscibility.[4,5] In this miscible system, the solid (liquid) state is a phase of variable composition. The composition variation allows one to obtain intermediate properties between the material properties of the initial compounds. Due to miniaturization, there is strong interest to investigate the properties of these materials at the nanoscale. In this paper, we report a theoretical investigation, free of any adjustable parameters, concerning the size and shape effects on the melting temperature, energy band gap, and phase diagrams of these III-V nanomaterials. A possible surface segregation is also considered. This study is particularly helpful to tune the thermal and optical properties of these compounds with size and composition. First of all, we restrict our discussion to binary and ternary III-V semiconductors with a zinc-blende crystal structure, i.e., phosphides, arsenides, and antimonides.

II. THEORETICAL DETERMINATION OF THE MELTING TEMPERATURE OF PHOSPHIDE, ARSENIDE, AND ANTIMONIDE III-V NANOMATERIALS

Since the pioneering work of Pawlow[6] in 1909, many models describe the variation in the melting temperature with the particle size.[7–25] This behavior is explained by the particular role played by the surface at the nanoscale.[26] Indeed when the size decreases, the number of atoms at the surface is no longer negligible compared to the number of atoms in the (bulk) volume. To study the melting temperature at the nanoscale, there are two approaches currently used: top-down and bottom-up. The first makes use of classical thermodynamics,[6,8–20] whereas the second relies on computational methods such as molecular dynamics.[21–25] Molecular dynamics generally considers less than 10^5 atoms in order to keep calculation times within reasonable values.[25] This factor limits the nanostructure size modeled to a maximum size of tens of nanometers; on the other hand, effects such as chemical environment on the melting temperature can be considered. Therefore, the top-down approach where one can consider longer particles emerges as a simple complementary method that may provide useful insights in nanotechnology.[17–19,27–31] One should note that thermodynamics as a phenomenological theory is strictly valid for macroscopic systems; therefore, it is necessary to obtain a statistical limit of validity in terms of size for classical thermodynamics, considering that the relative temperature fluctuation inside a sphere $\delta T/T \approx (nV)^{-1/2}$ (where V is the volume of the sphere with n atoms per unit volume) is around 2% for a radius $\sim$2 nm. This is the lower size limit that we will use for this work. Therefore any shape instability effects due to the thermal fluctuations above 2% are not addressed here, and other methods such as molecular-dynamics simulations should be considered for such extremely small nanostructures (<2 nm) or clusters of atoms.

We adopt the top-down approach using classical thermodynamics. The reasoning is based on the calculation of the temperature variation in the Gibbs free energy of the liquid phase, $G_l(T)$, relative to that of the solid phase, $G_s(T)$. At a fixed temperature, the Gibbs free-energy difference of a nanoparticle is expressed as $G_l - G_s = G_{l,\infty} - G_{s,\infty} + (A/V)(\gamma_l - \gamma_s)$. The phase transition occurs when $G_l - G_s = 0$. The melting temperature at the nanoscale, T_m, for free-standing nanostructures can be expressed as function of the bulk melting temperature, $T_{m,\infty}$, the size of the structure and one shape parameter.[13,17–19,28,29]

 ©2009 The American Physical Society

TABLE I. Bulk material properties of zinc-blende III-V semiconductors. The melting temperature, energy band gap, and surface energy in the liquid and solid phases, the melting enthalpy, and the exciton Bohr radius are indicated.

Material	$T_{m,\infty}$ (K)	$E_{g,\infty}$ (eV)	γ_l (Jm^{-2})	γ_s (Jm^{-2})	$\Delta H_{m,\infty}$ 10^9(Jm^{-3})	a_B (nm)
AlP	2100[e]	2.450 I[b]	0.566 ± 0.060[a]	1.096[c]	8.43[d]	1.2[f]
	2823[d]					
GaP	1749[d,g]	2.272 I[b]	0.510 ± 0.060[a]	0.962[c]	5.07[d,h]	7.3[f]
InP	1343[i]	1.344 D[b]	0.385[j]	0.755[c]	2.71[d]	16.8[f]
	1327[d]				3.47[k]	
	1330[e]					
AlAs	2013[d,e]	2.153 I[b]	0.506 ± 0.060[a]	0.897[c]	5.30[d]	2.0[f]
GaAs	1510[e,g]	1.424 D[b]	0.470[j,l]	0.860[g]	3.22[g]	12.3[f]
	1511[d]				3.86[d]	
InAs	1215[d,e,g]	0.354 D[b]	0.392[j,l]	0.656[g]	2.31[g]	35.0[f]
					2.38[d]	
AlSb	1330[e]	1.615 I[b]	0.441 ± 0.060[a]	0.682[c]	2.29[d]	2.7[f]
	1338[d]				1.66[i]	
GaSb	976[i]	0.750 D[b]	0.440[j]	0.632[c]	1.95[d]	22.0[f]
	980[e]				0.79[i]	
	985[d]					
InSb	798[e,i]	0.230 D[b]	0.290[j]	0.528[c]	1.32[d]	68.0[f]
	800[d]				0.70[i]	

[a]Calculated by this work.
[b]Reference 3.
[c]Reference 39.
[d]Reference 47.
[e]Reference 51.
[f]Reference 52.
[g]Reference 53.
[h]Reference 54.
[i]Reference 55.
[j]Reference 56.
[k]Reference 57.
[l]Reference 58.

$$\frac{T_m}{T_{m,\infty}} = 1 - \frac{\alpha_{\text{shape}}}{2L}, \tag{1}$$

where the shape parameter α_{shape} is defined as $\alpha_{\text{shape}} = 2AL(\gamma_s - \gamma_l)/(V\Delta H_{m,\infty})$, where L is the smallest dimension of the structure (i.e., for a sphere $L=R$). For free-standing nanoparticles, the sphere has the lowest α_{shape}. In case of polyhedral nanoparticles, the more faces you have on the nanoparticle, the higher is the value of α_{shape}. Therefore for a given size of nanoparticle, the nanoscale melting temperature is higher for the sphere compared to the other shapes. It means a higher thermal stability for spherical free-standing nanoparticles due to Gibbs' energy minimization. A (m^2) and V (m^3) are the surface area and volume of the nanostructure, respectively. $\Delta H_{m,\infty}$ is the bulk melting enthalpy (J/m^3), whereas γ_l and γ_s are the surface energy in the liquid and solid phases (J/m^2), respectively. γ_l and γ_s are considered size independent. This is justified by the fact that the size effect on the surface energies is less than 4% for sizes higher than 4 nm.[32–35] These material properties are indicated for III-V semiconductors in Table I.

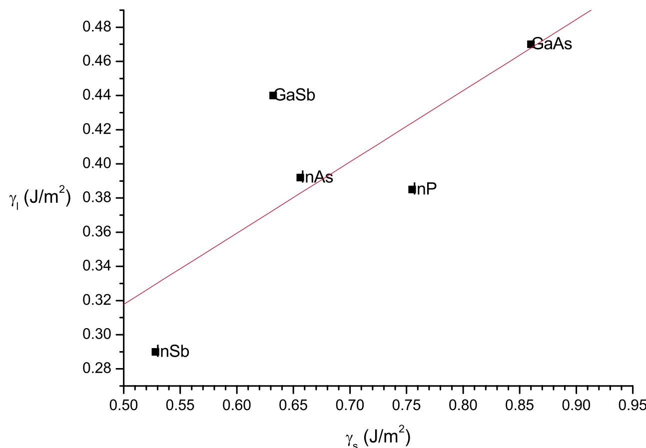

FIG. 1. (Color online) Surface energy in the liquid state versus the surface energy in the solid state for the III-V semiconductors.

III. THEORETICAL DETERMINATION OF THE ENERGY BAND GAP OF PHOSPHIDE, ARSENIDE, AND ANTIMONIDE III-V NANOMATERIALS

The energy band gap is well known to be temperature dependent.[36,37] The energy band gap of semiconductors increases when the temperature is decreased ($E_g = \Delta H_{\text{cv}} - T\Delta S_{\text{cv}}$). ΔH_{cv} and ΔS_{cv} represent the enthalpy and entropy variation between the conduction and valence electronic

TABLE II. The shape parameters of the zinc-blende III-V semiconductors are given for the sphere.

α_{sphere} (nm)	P	As	Sb
Al	0.38	0.44	0.63–0.87
Ga	0.54	0.61–0.73	0.59–1.46
In	0.64–0.82	0.67–0.69	1.08–2.05

bands. This behavior can be better understood if one considers that the interatomic spacing decreases when the amplitude of the atomic vibrations decreases due to the decreased thermal energy. A decreased interatomic spacing increases the potential seen by the electrons in the material, which in turn increases the size of the energy band gap. Therefore such temperature-dependent property is also size dependent due to the size effect on the melting temperature [Eq. (1)]. Indeed, the melting temperature indicates the maximal temperature accessible by a solid nanostructure; therefore when L decreases, the limit temperature T decreases also ($T \propto 1-\alpha_{\text{shape}}/2L$) which increases E_g ($E_g \propto -T$). Explicitly, using the Li's equation $(E_g - E_{g,\infty})/E_{g,\infty} = 1 - T_m/T_{m,\infty}$,[38] this means that with the same α_{shape} parameter, we can describe the size effect on the energy band gap of semiconductors, E_g, with the following equation:[30]

$$\frac{E_g}{E_{g,\infty}} = 1 + \frac{\alpha_{\text{shape}}}{2L}, \tag{2}$$

where $E_{g,\infty}$ is the energy band gap of the bulk semiconductor.

IV. THEORETICAL DETERMINATION OF THE UNKNOWN SURFACE ENERGY IN THE LIQUID STATE OF GaP, AlP, AlAs, AND AlSb

From Secs. II and III, it is clear that the surface plays a major role in nano- and microtechnology, especially in the determination of the melting temperature and energy band gap of nanostructures. Therefore, it is important to evaluate the unknown surface energies in liquid state of GaP, AlP, AlAs, and AlSb. Here, we propose a smart way to reach this issue by analyzing the properties of phosphides, arsenides, and antimonides III-V semiconductors.

From Table I, it is interesting to note that for aluminum,

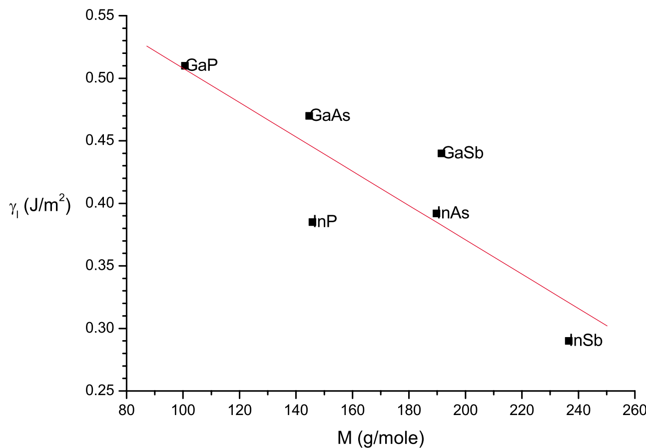

FIG. 2. (Color online) Surface energy in the liquid state versus the molar mass of the III-V semiconductors.

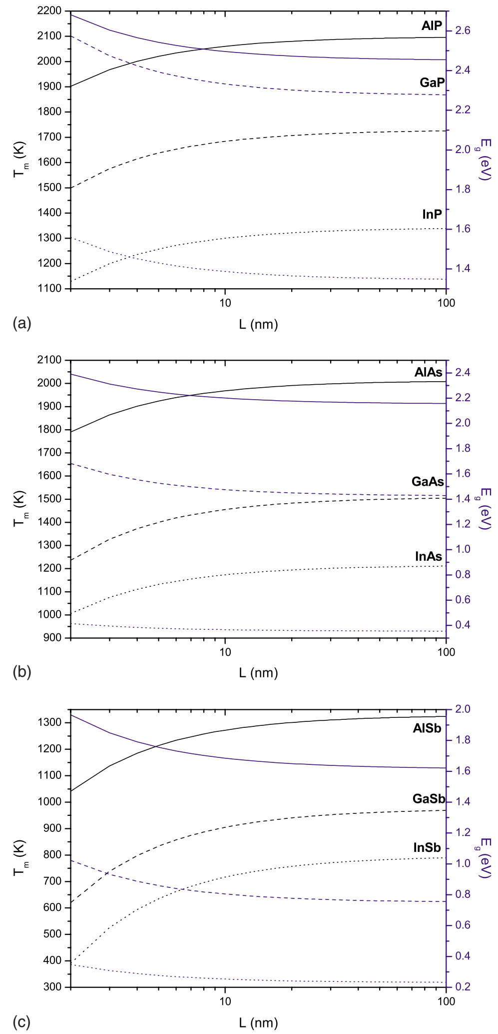

FIG. 3. (Color online) (a) The melting temperature [calculated with Eq. (1)] and the energy band gap [calculated with Eq. (2)] versus the radius (L) of spherical nanoparticle of AlP, GaP, and InP. The solid lines and dashed and dotted lines correspond to AlP, GaP, and InP, respectively. The colors are used to distinguish the melting temperature in black from the energy band gap in blue. (b) The melting temperature [calculated with Eq. (1)] and the energy band gap [calculated with Eq. (2)] versus the radius (L) of spherical nanoparticle of AlAs, GaAs, and InAs. The solid lines and dashed and dotted lines correspond to AlAs, GaAs, and InAs, respectively. The colors are used to distinguish the melting temperature in black from the energy band gap in blue. (c) The melting temperature [calculated with Eq. (1)] and the energy band gap [calculated with Eq. (2)] versus the radius (L) of spherical nanoparticle of AlSb, GaSb, and InSb. The solid lines, dashed and dotted lines correspond to AlSb, GaSb, and InSb, respectively. The colors are used to distinguish the melting temperature in black from the energy band gap in blue.

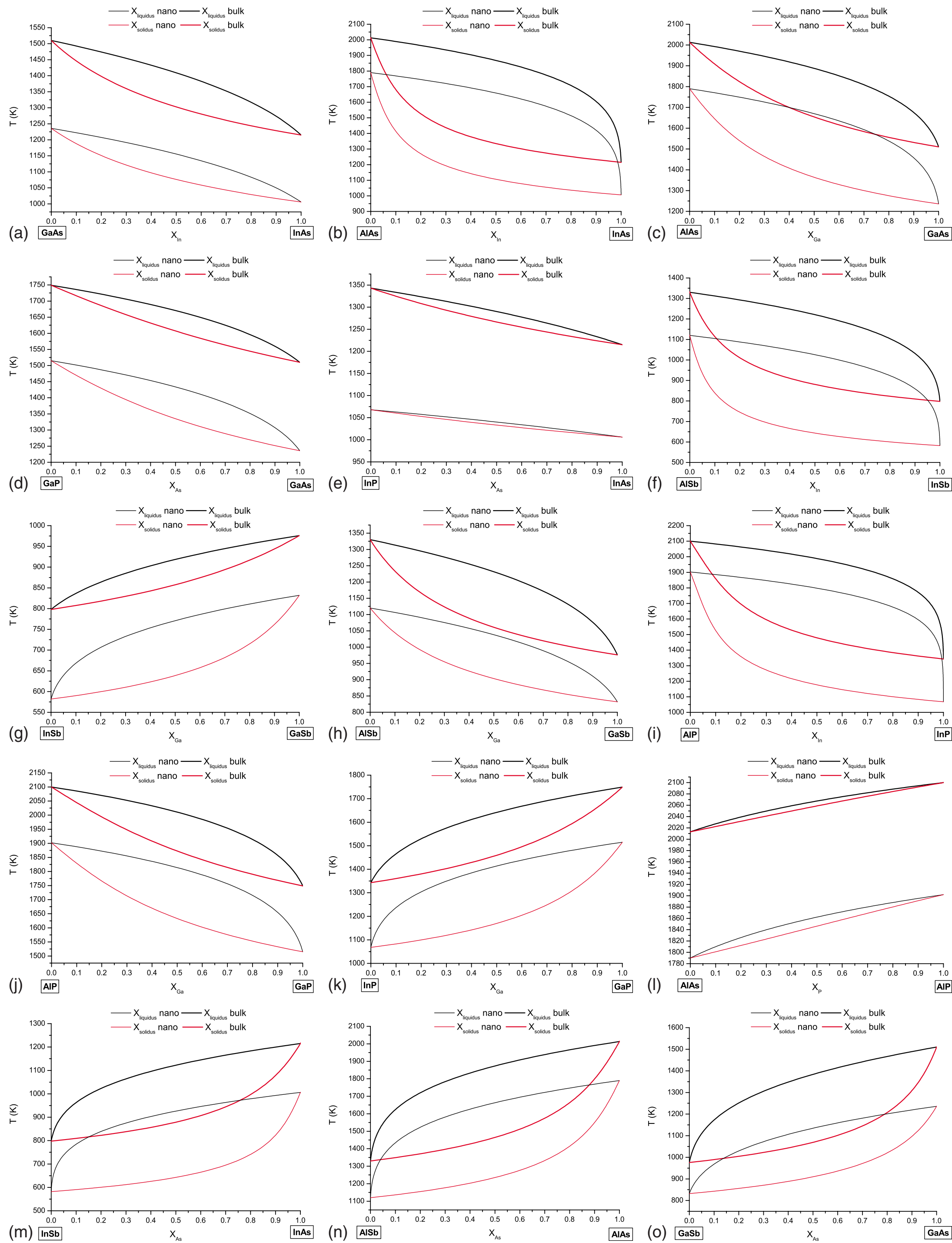

FIG. 4. (Color online) Phase diagram of III-V miscible semiconductors. The solidus (red) and liquidus (black) curves are indicated for the bulk material (thick lines) and the spherical nanomaterial (thin lines) with a radius equal to 2 nm and without segregation [calculated with Eq. (5)].

gallium, and indium compounds, the surface energy in the liquid state increased from antimonide to arsenide and phosphides as already observed by Liu *et al.*[39] Therefore, we can expect a surface energy value for GaP higher than 0.470 $\mathrm{J/m^2}$. From the material data announced in Table I, the liquid surface energy has been plotted versus the solid surface energy in Fig. 1. The relation between the surface energies can be determined by the following equation:

$$\gamma_l = 0.109\,28 + 0.416\,97\gamma_s, \tag{3}$$

where γ_l and γ_s are both expressed in $\mathrm{J/m^2}$.

Therefore, the surface tension of GaP is calculated to be $0.510 \pm 0.067\ \mathrm{J/m^2}$. To validate this result let us calculate the α_{shape} in a case of a spherical nanoparticle for the following compounds: InP, InAs, InSb, GaAs, and GaSb. The results are indicated in Table II. From it, we can see that gen-

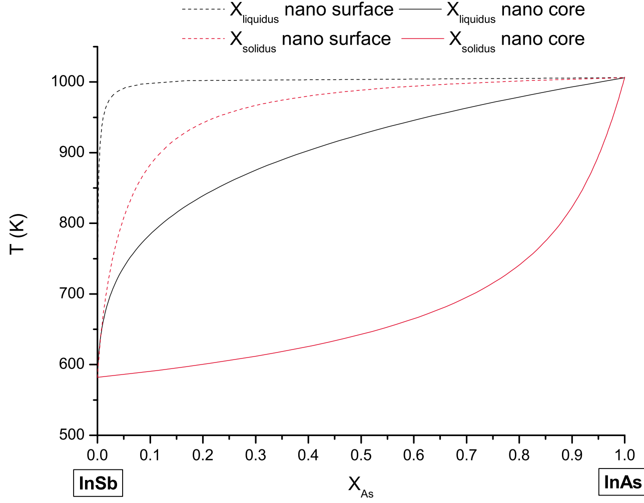

FIG. 5. (Color online) Phase diagram of the InAsSb alloy considering the segregation effect. To plot the graph, we take $\Delta H_{sub} \approx \Delta H_{vap} = 5$ kT. The solid lines correspond to the nanocore, and the dashed lines correspond to the nanosurface. The solidus and liquidus curves are indicated in red and black, respectively.

erally the α_{sphere} parameter follows the following relation: $\alpha_{sphere}(XP) < \alpha_{sphere}(XAs) < \alpha_{sphere}(X\text{Sb})$, where X design aluminum, gallium, or indium element. Therefore, the α_{sphere} parameter of GaP has to be lower than the α_{sphere} parameter of GaAs which is equal to 0.73 nm. From Eq. (1) or (2), we can deduce a lower limit of the GaP surface tension: $\gamma_l(\text{GaP}) \geq 0.344$ J/m^2. Let us remember that for a given material, the liquid surface energy is always lower than the solid surface energy, then we have $\gamma_l(\text{GaP}) \leq 0.962$ J/m^2. Therefore, we restrict the GaP liquid surface energy between: $0.344\ \text{J/m}^2 \leq \gamma_l(\text{GaP}) \leq 0.962\ \text{J/m}^2$ which is in agreement with the value calculated by Eq. (3).

By plotting in Fig. 2 the surface energy in the liquid state versus the molar mass, it is possible to determine from the linear fit given by Eq. (4) the surface energy in the liquid state for AlP, AlAs, and AlSb compounds (Table I);

$$\gamma_l = 0.645\,22 - 0.001\,37\ M, \tag{4}$$

where γ_l is expressed in J/m^2 and M is expressed in g/mol.

V. THEORETICAL PHASE DIAGRAMS OF PHOSPHIDE, ARSENIDE, AND ANTIMONIDE III-V NANOMATERIALS

To the best of our knowledge, there are no papers discussing the size effect on the phase diagram of the miscible III-V semiconductors. According Refs. 1, 4, 40, and 41, InAs-GaAs, InAs-AlAs, InAs-InP, GaAs-AlAs, GaAs-GaP, AlAs-AlP, InSb-GaSb, InSb-AlSb, GaSb-AlSb, InP-GaP, InP-AlP, GaP-AlP, InAs-InSb, GaAs-GaSb, and AlAs-AlSb are totally miscible; therefore, we can apply the assumption of ideal solutions. Considering no surface segregation, in the case of ideal solutions, the liquidus and solidus curves are calculated from the two simultaneous equations obtained by expressing the equality of the chemical potential in the two phases.[18,19,42]

TABLE III. Bowing parameter of the considered III-V ternary alloys. x designs the composition.

Material	C (eV)[a]
InGaAs	0.477
InAlAs	0.70
InAsSb	0.67
InAsP	0.10
GaAlAs	$-0.127+1.310x$
GaAsSb	1.43
GaAsP	0.19
AlAsSb	0.8
AlAsP	0.22
InGaSb	0.415
InAlSb	0.43
GaAlSb	$-0.044+1.22x$
InGaP	0.65
InAlP	-0.48
GaAlP	0

[a]Reference 2.

$$\begin{cases} kT\ln\left(\dfrac{x_{\text{solidus}}}{x_{\text{liquidus}}}\right) = \Delta H_m^A\left(1-\dfrac{T}{T_m^A}\right), \\ kT\ln\left(\dfrac{1-x_{\text{solidus}}}{1-x_{\text{liquidus}}}\right) = \Delta H_m^B\left(1-\dfrac{T}{T_m^B}\right), \end{cases} \tag{5}$$

where x_{solidus} (x_{liquidus}) is the composition in the solid (liquid) phase at a given T, respectively. T_m^i is the melting temperature of the element i. ΔH_m^i is the melting enthalpy of the element i.

According to Ref. 43, the size effect on the melting enthalpy can be calculated by $\Delta H_m / \Delta H_{m,\infty} = T_m / T_{m,\infty}$. Let us now consider a possible surface segregation. It refers to the phenomenon by which the chemical composition at the surface of alloys differs from the composition in the core. Nanoalloys have the particularity to accommodate on the surface the structural defects introduced by the stoichiometric deviations. According to Williams and Nason,[44] the surface compositions of the liquid and solid phase are given by

$$\begin{cases} x_{\text{solidus}}^{\text{surface}} = \dfrac{(x_{\text{solidus}}/1-x_{\text{solidus}})e^{-(\Delta H_{\text{sub}}z_{1v})/(z_1kT)}}{1+(x_{\text{solidus}}/1-x_{\text{solidus}})e^{-(\Delta H_{\text{sub}}z_{1v})/(z_1kT)}}, \\ x_{\text{liquidus}}^{\text{surface}} = \dfrac{(x_{\text{liquidus}}/1-x_{\text{liquidus}})e^{-(\Delta H_{\text{vap}}z_{1v})/(z_1kT)}}{1+(x_{\text{liquidus}}/1-x_{\text{liquidus}})e^{-(\Delta H_{\text{vap}}z_{1v})/(z_1kT)}}, \end{cases} \tag{6}$$

where z_1 is the first nearest-neighbor atoms. z_{1v} is the number of first nearest atoms above the same plane (vertical direction). In the case of the zinc-blende crystal structure, we have $z_1=4$ and $z_{1v}=3$. ΔH_{vap} is the difference between the vaporization enthalpies of the two pure elements, $\Delta H_{\text{vap}} = \Delta H_v^A - \Delta H_v^B$. ΔH_{sub} is the difference between the sublimation enthalpies of the two pure elements, $\Delta H_{\text{sub}} = \Delta H_s^A - \Delta H_s^B$. Ele-

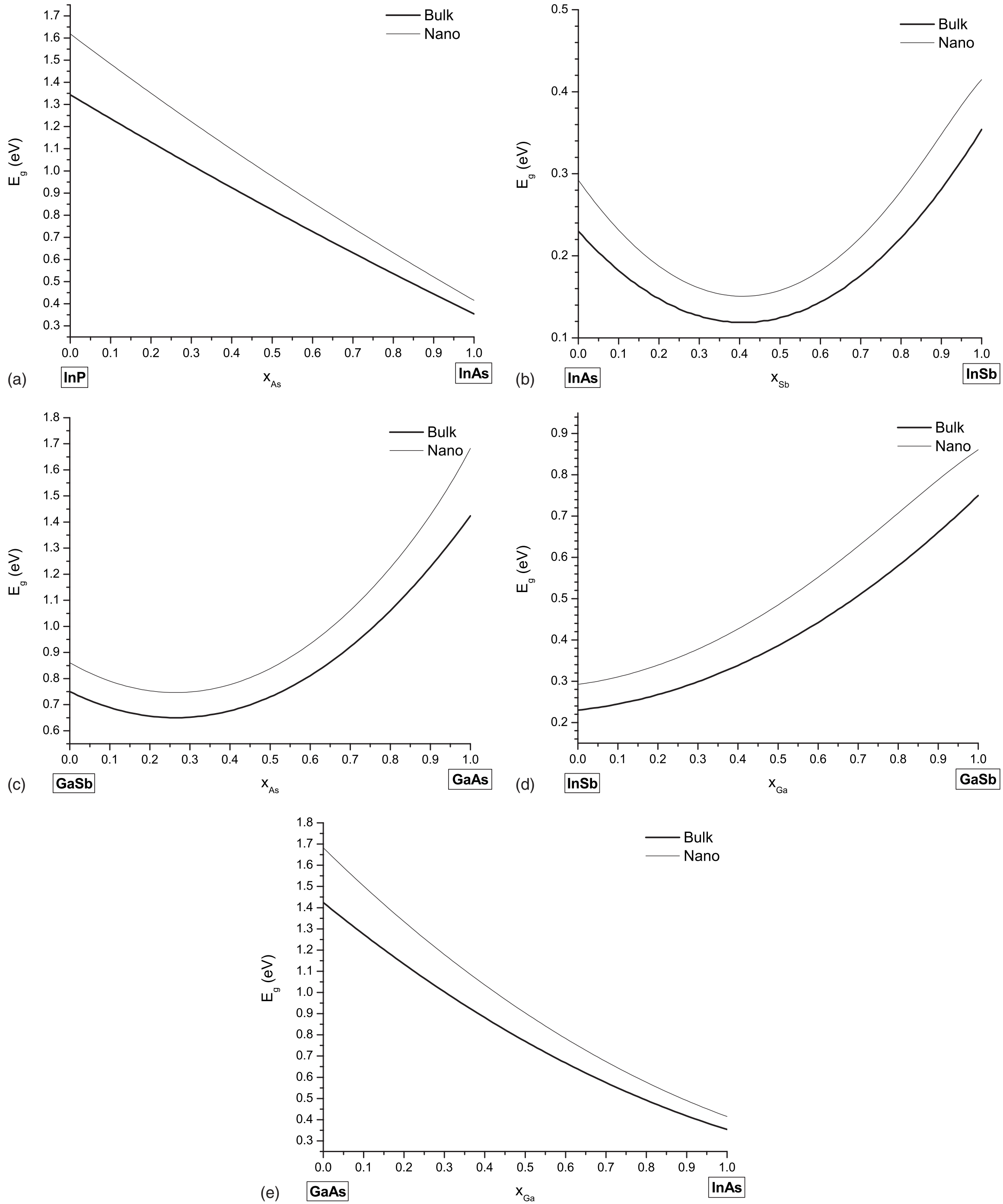

FIG. 6. Direct energy band gap versus the composition of the alloy (a) InAsP, (b) InAsSb, (c) GaAsSb, (d) InGaSb, and (e) InGaAs. The thick line indicates the bulk behavior, and the thin one indicates the spherical nanomaterial behavior with a radius equal to 2 nm and without segregation.

ment A is chosen to be the one with the highest sublimation and vaporization enthalpies. If the two components are identical, $\Delta H_{sub}=0$ and $\Delta H_{vap}=0$, there is no segregation and we retrieve Eq. (5). $x_{solidus}$ and $x_{liquidus}$ are obtained from solving Eq. (5).

VI. DISCUSSION

First of all, we can observe in Table I among the III-V semiconductors when the molar mass increases the melting temperature, the energy band gap, the surface energy in the liquid (solid) state, and the melting enthalpy decrease. Among III-V phosphides, the atomic Bohr radius increases when the molar mass increases as well as for arsenides and antimonides.

Figures 3(a)–3(c) show the size effect on the melting temperature of spherical III-P, III-As, and III-Sb nanoparticles. Note that our results obtained by Eq. (1) use isotropic values for the solid surface energy instead of better information. In

Fig. 3, we can also see the size effect on the energy band gap of III-V semiconductors spherical nanoparticles. The predicted values are in relative good agreement with the experimental and calculated values announced in Refs. 45 and 46. Let us pay attention to quantum effects appearing for sizes below Bohr radius, a_B. Indeed quantum confinement will play a role when $L \leq a_B$, and therefore care has to be taken during the comparison between our theoretical results with optical measurements subjected to quantum confinement. Nevertheless, our theory can be applied below a_B.

Figure 4 represents the phase diagrams of the considered III-V semiconductors for the bulk and the spherical nanomaterial with a radius equal to 2 nm. The general lens shape of the liquidus-solidus curves is conserved. Considering the bulk vaporization enthalpy of InAs and InSb (5.64 and 5.51 eV/atom, respectively)[47] in Eq. (6) instead of better information concerning the nanoscaled vaporization enthalpy, let us now evaluate the segregation effect on the InAsSb alloy. This is shown in Fig. 5. The lens shape of the liquidus/solidus curves is deformed. The liquidus and solidus curves at the surface are depleted of the higher bond energy element, in this case As. This result is in agreement with Ref. 48. Therefore, it means that we have more InSb at the surface than in the core, and it can explain the surface melting phenomena $[T_m^{\mathrm{InSb}}(L) < T_m^{\mathrm{InAs}}(L)]$, which means that the surface melts first due to the core-shell structure obtained with segregation. Indeed, the segregation is responsible of the core-shell structure generally met in nanostructures.[49] As announced by Liang *et al.*,[50] we also observed in Fig. 5 that the two-phase zone generally decreases as the size decreases, which is due to the size effect on the melting enthalpy.

From the phase diagram, it is possible to deduce the variation in the energy band gap of a nanostructure versus its composition. By a polynomial fit of the solidus curve, we can get the variation in the melting temperature with its composition to evaluate the variation in the α_{shape} parameter with the composition. Then with Eqs. (2) and (7), we can evaluate the variation in the energy band gap of the nanostructure with its composition. Equation (7) describes the energy band-gap behavior of the bulk as function of its composition,

$$E_{g,\infty}(A_{1-x}B_x) = (1-x)E_{g,\infty}(A) + xE_{g,\infty}(B) - x(1-x)C, \tag{7}$$

where A and B represent the two binary compounds. C is the bowing parameter which is indicated in Table III. x is the composition. This is shown in Fig. 6, for example, for direct energy band-gap semiconductors.

VII. CONCLUSIONS

To conclude, we have studied the size, shape, composition, and segregation effects on the melting temperature, energy band gap, and phase diagrams of miscible III-V semiconductors within a thermodynamical approach. The phase diagrams of the following semiconducting alloys were plotted for the first time at the nanoscale. Some deviations from our predictions are expected for sizes below Bohr radius because quantum confinement has to be considered to be compared with optical measurements. Moreover, careful experimental determination of the melting, vaporization, and sublimation enthalpies is needed to fully apply Eq. (6). A slight error in the determination of these values can be dramatic in the evaluation of the phase diagrams because these values are involved in the exponential factors of Eqs. (5) and (6). Finally, these thermodynamic considerations developed in this communication can assist to the tuning of the semiconductors optical properties.

ACKNOWLEDGMENTS

G.G. thanks the ANR PNANO M&NEMS project for financial support.

*Corresponding author. gregory.guisbiers@physics.org

[1] *Numerical Data and Functional Relationships in Science and Technology*, edited by O. Madelung, Landolt-Börnstein, New Series, Group III, Vol. 17, Pt. A (Springer-Verlag, Berlin, 1982).
[2] I. Vurgaftman, J. R. Meyer, and L. R. Ram-Mohan, J. Appl. Phys. **89**, 5815 (2001).
[3] U. K. Mishra and J. Singh, *Semiconductor Device Physics and Design* (Springer, Dordrecht, 2008).
[4] E. K. Müller and J. L. Richards, J. Appl. Phys. **35**, 1233 (1964).
[5] M. Ilegems and G. L. Pearson, Annu. Rev. Mater. Sci. **5**, 345 (1975).
[6] P. Pawlow, Z. Phys. Chem., Stoechiom. Verwandtschaftsl. **65**, 1 (1909).
[7] D. Ganguli, Trans. Indian Ceram. Soc. **67**, 49 (2008).
[8] P. Buffat and J. P. Borel, Phys. Rev. A **13**, 2287 (1976).
[9] P. R. Couchman and W. A. Jesser, Nature (London) **269**, 481 (1977).
[10] J. P. Borel, Surf. Sci. **106**, 1 (1981).
[11] A. N. Goldstein, C. M. Echer, and A. P. Alivisatos, Science **256**, 1425 (1992).
[12] M. Wautelet, J. Phys. D **24**, 343 (1991).
[13] M. Wautelet, Phys. Lett. A **246**, 341 (1998).
[14] M. Zhao, X. H. Zhou, and Q. Jiang, J. Mater. Res. **16**, 3304 (2001).
[15] Z. Zhang, M. Zhao, and Q. Jiang, Semicond. Sci. Technol. **16**, L33 (2001).
[16] K. K. Nanda, S. N. Sahu, and S. N. Behera, Phys. Rev. A **66**, 013208 (2002).
[17] G. Guisbiers and M. Wautelet, Nanotechnology **17**, 2008 (2006).
[18] G. Abudukelimu, G. Guisbiers, and M. Wautelet, J. Mater. Res. **21**, 2829 (2006).
[19] G. Guisbiers, G. Abudukelimu, F. Clement, and M. Wautelet, J. Comput. Theor. Nanosci. **4**, 309 (2007).
[20] A. Safaei, M. A. Shandiz, S. Sanjabi, and Z. H. Barber, J. Phys.: Condens. Matter **19**, 216216 (2007).
[21] C. Q. Sun, B. K. Tay, X. T. Zeng, S. Li, T. P. Chen, J. Zhou, H. L. Bai, and E. Y. Jiang, J. Phys.: Condens. Matter **14**, 7781 (2002).

[22] C. Q. Sun, Prog. Solid State Chem. **35**, 1 (2007).
[23] J. L. Rodriguez-Lopez, J. M. Montejano-Carrizales, and M. José-Yacaman, Appl. Surf. Sci. **219**, 56 (2003).
[24] F. Ding, A. Rosen, S. Curtarolo, and K. Bolton, Appl. Phys. Lett. **88**, 133110 (2006).
[25] F. Delogu, Nanotechnology **18**, 325706 (2007).
[26] Q. S. Mei and K. Lu, Prog. Mater. Sci. **52**, 1175 (2007).
[27] G. Guisbiers, O. Van Overschelde, and M. Wautelet, Acta Mater. **55**, 3541 (2007).
[28] G. Guisbiers and S. Pereira, Nanotechnology **18**, 435710 (2007).
[29] G. Guisbiers, M. Kazan, O. Van Overschelde, M. Wautelet, and S. Pereira, J. Phys. Chem. C **112**, 4097 (2008).
[30] G. Guisbiers, O. Van Overschelde, and M. Wautelet, Appl. Phys. Lett. **92**, 103121 (2008).
[31] M. Wautelet and D. Duvivier, Eur. J. Phys. **28**, 953 (2007).
[32] L. H. Liang, M. Zhao, and Q. Jiang, J. Mater. Sci. Lett. **21**, 1843 (2002).
[33] R. C. Tolman, J. Chem. Phys. **17**, 333 (1949).
[34] H. M. Lu and Q. Jiang, J. Phys. Chem. B **108**, 5617 (2004).
[35] Z. Zhang, X. X. Lü, and Q. Jiang, Physica B **270**, 249 (1999).
[36] S. P. Keller, *Handbook on Semiconductors: Materials, Properties and Preparation* (North-Holland, Amsterdam, 1980), Vol. 3.
[37] J. A. Van Vechten and M. Wautelet, Phys. Rev. B **23**, 5543 (1981).
[38] M. Li and J. C. Li, Mater. Lett. **60**, 2526 (2006).
[39] W. Liu, W. T. Zheng, and Q. Jiang, Phys. Rev. B **75**, 235322 (2007).
[40] G. B. Stringfellow, J. Phys. Chem. Solids **33**, 665 (1972).
[41] W. A. Jesser and C. T. Schamp, Phys. Status Solidi C **5**, 539 (2008).
[42] R. Vallée, M. Wautelet, J. P. Dauchot, and M. Hecq, Nanotechnology **12**, 68 (2001).
[43] G. Guisbiers and L. Buchaillot, J. Phys. Chem. C **113**, 3566 (2009).
[44] F. L. Williams and D. Nason, Surf. Sci. **45**, 377 (1974).
[45] C. C. Yang and S. Li, J. Phys. Chem. C **112**, 2851 (2008).
[46] J. Li and L.-W. Wang, Phys. Rev. B **72**, 125325 (2005).
[47] *Numerical Data and Functional Relationships in Science and Technology*, edited by O. Madelung, U. Rössler, and M. Schulz, Landolt-Börnstein, New Series, Group III, Vol. 41, Pt. A1b (Springer-Verlag, Berlin, 2002).
[48] J.-H. Cho, S. B. Zhang, and A. Zunger, Phys. Rev. Lett. **84**, 3654 (2000).
[49] S. Xiao, W. Hu, W. Luo, Y. Wu, X. Li, and H. Deng, Eur. Phys. J. B **54**, 479 (2006).
[50] L. H. Liang, D. Liu, and Q. Jiang, Nanotechnology **14**, 438 (2003).
[51] http://www.matweb.com
[52] *Numerical Data and Functional Relationships in Science and Technology*, edited by C. Klingshirn, Landolt-Börnstein, New Series, Group III, Vol. 34, Pt. C1 (Springer-Verlag, Berlin, 2001).
[53] W. Martienssen and H. Warlimont, *Springer Handbook of Condensed Matter and Materials Data* (Springer, Berlin, 2005).
[54] D. R. Vij, *Handbook of Electroluminescent Materials* (IOP, London, 2004).
[55] D. L. Perry and S. L. Phillips, *Handbook of Inorganic Compounds* (CRC, Boca Raton, 1995).
[56] S. Nakamura and T. Hibiya, Int. J. Thermophys. **13**, 1061 (1992).
[57] R. B. Bird, W. E. Stewart, and E. N. Lightfoot, *Transport Phenomena* (Wiley, New York, 1960).
[58] M. D. Amashukeli, V. V. Karataev, M. G. Kekua, M. G. Mil'vidskii, and D. V. Khantadze, Neorg. Mater. **17**, 2126 (1981).